ORIGINAL PAPER

Comparison of shear and compression jammed packings of frictional disks

Fansheng Xiong[1,2] · Philip Wang[2] · Abram H. Clark[3] · Thibault Bertrand[4] · Nicholas T. Ouellette[5] · Mark D. Shattuck[6] · Corey S. O'Hern[2,7,8]

Abstract

We compare the structural and mechanical properties of mechanically stable (MS) packings of frictional disks in two spatial dimensions (2D) generated with isotropic compression and simple shear protocols from discrete element modeling (DEM) simulations. We find that the average contact number and packing fraction at jamming onset are similar (with relative deviations < 0.5%) for MS packings generated via compression and shear. In contrast, the average stress anisotropy $\langle \hat{\Sigma}_{xy} \rangle = 0$ for MS packings generated via isotropic compression, whereas $\langle \hat{\Sigma}_{xy} \rangle > 0$ for MS packings generated via simple shear. To investigate the difference in the stress state of MS packings, we develop packing-generation protocols to first unjam the MS packings, remove the frictional contacts, and then rejam them. Using these protocols, we are able to obtain rejammed packings with nearly identical particle positions and stress anisotropy distributions compared to the original jammed packings. However, we find that when we directly compare the original jammed packings and rejammed ones, there are finite stress anisotropy deviations $\Delta \hat{\Sigma}_{xy}$. The deviations are smaller than the stress anisotropy fluctuations obtained by enumerating the force solutions within the null space of the contact networks generated via the DEM simulations. These results emphasize that even though the compression and shear jamming protocols generate packings with the same contact networks, there can be residual differences in the normal and tangential forces at each contact, and thus differences in the stress anisotropy.

1 Introduction

Granular materials, which are collections of macroscopic-sized grains, can exist in fluidized states when the applied stress exceeds the yield stress or in solid-like, or jammed, states when the applied stress is below the yield stress [1, 2]. Many recent studies [3–8] have shown that the structural and mechanical properties of jammed granular packings depend on the protocol that was used to generate them. For example, when granular packings are generated via simple or pure shear, the force chain networks appear more heterogeneous and anisotropic. In contrast, for granular packings

✉ Philip Wang
philip.wang@yale.edu

Corey S. O'Hern
corey.ohern@yale.edu

1 Zhou Pei-Yuan Center for Applied Mathematics, Tsinghua University, Beijing 100084, China

2 Department of Mechanical Engineering and Materials Science, Yale University, New Haven, CT 06520, USA

3 Department of Physics, Naval Postgraduate School, Monterey, CA 93943, USA

4 Department of Mathematics, Imperial College London, South Kensington Campus, London SW7 2AZ, England, UK

5 Department of Civil and Environmental Engineering, Stanford University, Stanford, CA 94305, USA

6 Benjamin Levich Institute and Physics Department, The City College of the City University of New York, New York, NY 10031, USA

7 Department of Physics, Yale University, New Haven, CT 06520, USA

8 Department of Applied Physics, Yale University, New Haven, CT 06520, USA

generated via isotropic compression, the force distribution is more uniform [9–13]. This protocol dependence for the structural and mechanical properties of jammed packings makes it difficult to accuccurate calculate, and even properly define, their statistical averages.

An important question to address when considering how to calculate statistical averages of a system's structural and mechanical properties is to determine which states are to be included in the statistical ensemble. For jammed granular packings, the relevant set of states is the collection of mechanically stable (MS) packings [14, 15] with force and torque balance on every grain. In addition, the average properties of the ensemble of MS packings depend on the probabilities with which each MS packing occurs, and the probabilities can vary strongly with the packing-generation protocol.

We recently investigated how the mechanical properties of granular systems composed of bidisperse frictionless disks interacting via pairwise, purely repulsive central forces [16] depend on the packing-generation protocol. In this case, the relevant ensemble of jammed states is the collection of isostatic MS packings [16–19] with $N_c = 2N' - 1$ interparticle contacts, where $N' = N - N_r$, N is the number of disks, and N_r is the number of rattler disks with less than 3 contacts. We compared MS packings of frictionless disks generated via simple or pure shear (i.e. shear jammed packings) and those generated via isotropic compression (i.e. compression jammed packings). We found that compression jammed packings can possess either positive or negative stress anisotropy $\hat{\Sigma}_{xy} = -\Sigma_{xy}/P$, where Σ_{xy} is the shear stress and P is the pressure of the MS packing. In contrast, shear jammed MS packings possess only $\hat{\Sigma}_{xy} > 0$ and these packings are identical to the MS packings generated via isotropic compression with $\hat{\Sigma}_{xy} > 0$. Thus, the ensemble of jammed packings generated via shear and isotropic compression is the same, but shear (in one direction) selects jammed packings with only one sign of the stress anisotropy.

In this article, we will investigate a similar question of whether exploring configuration space through shear versus through compression samples the same set of MS packings, except we consider the case of jammed packings of dry, frictional disks. A key feature of frictional systems is that the forces at each interparticle contact must obey the Coulomb condition [20, 21], where $f_{ij}^t \leq \mu f_{ij}^n$, f_{ij}^n and f_{ij}^t are the normal and tangential forces at the contact between particles i and j, and μ is the static friction coefficient. If f_{ij}^t exceeds μf_{ij}^n, the contact will slide to satisfy the Coulomb condition. Further, the number of contacts for MS packings of frictional disks is below the isostatic value $z_{iso} = 4$, and as a result there are many solutions for the normal and tangential forces for each fixed network of interparticle contacts. Thus, one can imagine that different protocols for generating jammed packings of frictional disks can give rise to MS packings with different distributions of sliding contacts, different force solutions for a given contact network, or even different types of contact networks.

We carry out discrete element modeling (DEM) simulations of bidipserse frictional disks in two dimensions (2D) to compare the properties of MS packings at jamming onset generated via simple shear and isotropic compression. We find five significant results: (1) The average packing fraction $\langle \phi_J(\mu) \rangle$ and contact number $\langle z_J(\mu) \rangle$ at jamming onset versus friction coefficient μ for the ensemble of MS packings generated via isotropic compression and simple shear are similar (with deviations $< 0.5\%$). In particular, both shear and compression jammed packings can possess a range of average contact numbers $\langle z_J \rangle$ between 3 and 4, depending on μ. (2) As with frictionless disks, we find that MS packings of frictional disks generated via isotropic compression possess both $\hat{\Sigma}_{xy} > 0$ and $\hat{\Sigma}_{xy} < 0$, whereas MS packings generated via simple shear possess only one sign of the stress anisotropy. (3) For each MS packing generated via simple shear, we can decompress the packing to remove all of the frictional contacts and recompress it to generate an MS packing with particle positions that are nearly identical to those of the original shear jammed MS packing. Similarly, for each MS packing generated via isotropic compression, we can shear it in a given direction to unjam it and remove all of the frictional contacts and shear it back in the opposite direction to generate an MS packing with disk positions that are nearly identical to those of the original compression jammed packing. (4) Even though the disk positions are nearly identical, we find a small, but significant difference between the stress anisotropy of the shear jammed packings and that for the compression rejammed packings. Similarly, we find a smaller, but significant difference in the stress anisotropy between the compression jammed packings and that for the shear rejammed packings. The fluctuations in the stress anisotropy between the originally jammed packings and the re-jammed packings from the DEM simulations are much smaller than the fluctuations obtained by enumerating all normal and tangential forces solutions from the null space for each fixed contact network. (5) We also show that even though we can generate MS packings with nearly identical particle positions via the DEM simulations with our rejamming protocols, the packings can possess very different mobility distributions $P(\xi)$, where $\xi = F_{ij}^t/\mu F_{ij}^n$, and numbers of sliding contacts. We find that deviations in the stress anisotropy can occur for packings with similar mobility distributions (i.e. between compression jammed and shear re-jammed packings) and for packings with different mobility distributions (i.e. between shear jammed and compression re-jammed packings). There are thus two key distinct contributions to the stress

anisotropy: the width of the distribution of stresses from the null space solutions and the distribution of sliding contacts.

The remainder of the article is organized as follows. The Methods section (Sect. 2) introduces the Cundall–Strack model [22] for static friction between disks, the definitions of the stress tensor, shear stress, and stress anisotropy, and the details of the isotropic compression and simple shear packing generation protocols. In addition, we describe the protocols to decompress and then recompress shear-jammed packings and shear unjam and then shear jam compression-jammed packings. The Results section (Sect. 3) describes our findings for the average packing fraction and contact number at jamming onset versus the static friction coefficient for MS packings generated via both protocols. In addition, we show the stress anisotropy and mobility distributions for each protocol that we use to generate MS packings. In the Conclusion and Future Directions section (Sect. 4), we summarize our results and describe promising future research directions, e.g. enuerating the force solutions for the null space of contact networks generated via isostropic compression and shear. In addition, we include three Appendices. In Appendix 1, we include calculations of the distribution of normal stress differences in shear and compression jammed packings. In Appendix 2, we provide the exact form of the jammed packing fraction versus shear strain for two bidisperse hard disks to motivate the parabolic form for geometrical families. In Appendix 3, we provide a sensitivity analysis for how the numerical parameters in the packing-generation protocols affect the extent to which shear and compression jammed packings can be unjammed and then re-jammed to reach the same particle positions and stress anisotropy of the original jammed packing.

2 Methods

We perform DEM simulations of frictional disks in 2D. We consider bidisperse mixtures of disks with $N/2$ large disks and $N/2$ small disks, each with the same mass m, and diameter ratio $\sigma_l/\sigma_s = 1.4$ [23]. The MS packings are generated inside a square box with side length L and periodic boundary conditions in both directions. The disks interact via pair forces in the normal (along the vector $\hat{r}_{ij}$ from the center of disk j to that of disk i) and the tangential $\hat{t}_{ij}$ directions (with $\hat{t}_{ij} \cdot \hat{r}_{ij} = 0$). We employ a repulsive linear spring potential for forces in the normal direction:

$$U^n(r_{ij}) = \frac{K\sigma_{ij}}{2}\left(1 - \frac{r_{ij}}{\sigma_{ij}}\right)^2 \theta\left(1 - \frac{r_{ij}}{\sigma_{ij}}\right), \tag{1}$$

where r_{ij} is the separation between disk centers, $\sigma_{ij} = (\sigma_i + \sigma_j)/2$, σ_i is the diameter of disk i, K is the spring constant in the normal direction, and $\theta(\cdot)$ is the Heaviside

step function that sets the interaction potential to zero when disks i and j are not in contact.

We implement the Cundall–Strack model [22] for the tangential frictional forces. When disks i and j are in contact, $\vec{f}_{ij}^t = K_t \vec{u}_{ij}^t$, where $K_t = K/3$ is the spring constant for the tangential forces and $\vec{u}_{ij}^t$ is the relative tangential displacement. $\vec{u}_{ij}^t$ is obtained by inegrating the relative tangential velocity [24, 25], while disks i and j are in contact:

$$\frac{d\vec{u}_{ij}^t}{dt} = \vec{v}_{ij}^t - \frac{(\vec{u}_{ij}^t \cdot \vec{v}_{ij})\vec{r}_{ij}}{r_{ij}^2}, \tag{2}$$

where $\vec{v}_{ij} = \vec{v}_i - \vec{v}_j$, $\vec{v}_{ij}^t = \vec{v}_{ij} - \vec{v}_{ij}^n - \frac{1}{2}(\vec{\omega}_i + \vec{\omega}_j) \times \vec{r}_{ij}$, $\vec{v}_{ij}^n = (\vec{v}_{ij} \cdot \hat{r}_{ij})\hat{r}_{ij}$, and $\vec{\omega}_i$ is the angular velocity of disk i. $\vec{u}_{ij}^t$ is set to zero when the pair of disks i and j is no longer in contact. We implement the Coulomb criterion, $f_{ij}^t \leq \mu f_{ij}^n$, by resetting $|\vec{u}_{ij}^t| = u_{ij}^t = \mu f_{ij}^n/K_t$ if f_{ij}^t exceeds μf_{ij}^n. The total potential energy is $U = U^n + U^t$, where $U^n = \sum_{i>j} U^n(r_{ij})$ and $U^t = \sum_{i>j} K_t(u_{ij}^t)^2/2$.

We characterize the stress of the MS packings using the virial expression for the stress tensor [16]:

$$\Sigma_{\beta\delta} = \frac{1}{A} \sum_{i>j} f_{ij\beta} r_{ij\delta}, \tag{3}$$

where $\beta, \delta = x, y$, $A = L^2$ is the area of the simulation box, $f_{ij\beta}$ is the β-component of the interparticle force $\vec{f}_{ij}$ on disk i due to disk j, and $r_{ij\delta}$ is the δ-component of the separation vector $\vec{r}_{ij}$. We define the stress anisotropy as $\hat{\Sigma}_{xy} = -\Sigma_{xy}/P$, the normal stress difference as $\hat{\Sigma}_N = (\Sigma_{yy} - \Sigma_{xx})/2P$, and the pressure as $P = (\Sigma_{xx} + \Sigma_{yy})/2$. We measure length, energy, and stress below in units of σ_s, $K\sigma_s$, and K/σ_s, respectively.

We employ two main protocols to generate MS packings: 1) isotropic compression at fixed shear strain γ and 2) simple shear at fixed packing fraction ϕ. (See Fig. 1.) For protocol 1 (isotropic compression), we first randomly place the disks in the simulation cell without overlaps. We then increase the diameters of the disks according to $\sigma_i' = \sigma_i(1 + d\phi/\phi)$ where $d\phi < 10^{-4}$ is the initial increment in the packing fraction. After each small change in packing fraction, we minimize the total potential energy U by adding viscous damping forces proportional to each disk's velocity $\vec{v}_i$. Energy minimization is terminated when $K_{max} < 10^{-20}$, where K_{max} is the maximum kinetic energy of one of the disks.

If $U/N < U_{tol}$ after minimization, we increase the packing fraction again by $d\phi$ and then minimize the total potential energy. To eliminate overlaps, we typically set $U_{tol} = 10^{-16}$, which means that the typical disk overlap is $< 10^{-8}$. If after minimization, $U/N > 2U_{tol}$, the growth step is too large and we return to the uncompressed packing of the previous step with $U/N < U_{tol}$. Instead, we increase the packing fraction by $d\phi/2$, and minimize the total potential energy. We
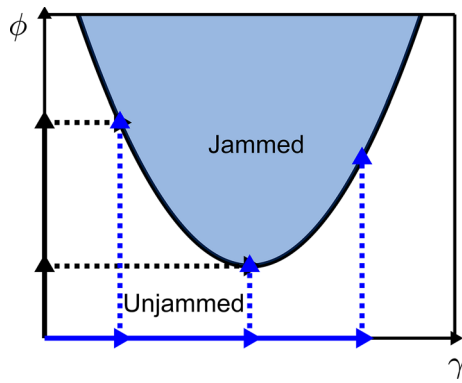
Fig. 1 An idealized jamming diagram in which the jammed and unjammed regions are separated by a parabolic boundary in the packing fraction ϕ and shear strain γ plane. For compression jamming, we first apply simple shear strain γ at $\phi = 0$ (horizontal solid blue lines) and then compress the system at fixed γ to jamming onset at ϕ_J (vertical dashed blue lines). For shear jamming, we first compress the system to $\phi < \phi_J$ (vertical solid black lines) and then apply simple shear to jamming onset at γ_J (horizontal dashed black lines) (color figure online)

repeat this process until the total potential energy satisfies $U_{\text{tol}} < U/N < 2U_{\text{tol}}$, at which we assume that the packing has reached jamming onset at packing fraction ϕ_J. This compression protocol ensures that the system approaches jamming onset from below.

For protocol 2, we first prepare the system below jamming onset at $\phi_t < \phi_J$ (using protocol 1). We then apply successive simple shear strain increments $d\gamma$ by shifting the disk positions, $x'_i = x_i + d\gamma y_i$, and implementing Lees-Edwards boundary conditions, which are consistent with the applied affine shear strain. The initial shear strain increment is $d\gamma = 10^{-4}$. After an applied shear strain increment, we minimize the total potential energy. Energy minimization is again terminated when $K_{\text{max}} < 10^{-20}$. If $U/N < U_{\text{tol}}$ after minimization, we increment the shear strain again by $d\gamma$ and minimize the total potential energy. If after minimization, $U/N > 2U_{\text{tol}}$, the shear strain step is too large and we return to the packing at the previous strain step with $U/N < U_{\text{tol}}$. Instead, we increment the shear strain by $d\gamma/2$, and minimize the total potential energy. We repeat this process until the total potential energy satisfies $U_{\text{tol}} < U/N < 2U_{\text{tol}}$, at which we assume that the packing has reached jamming onset at total shear strain γ_J.

Energy minimization is carried out by integrating Newton's equations of motion for the translational and rotational degrees of freedom of each disk in the presence of static friction and viscous dissipation. For the translational degrees of freedom, we have

$$m\frac{d^2\vec{r}_i}{dt^2} = \vec{f}_i^n + \vec{f}_i^t + \vec{f}_i^d, \tag{4}$$

where $\vec{f}_i^n = \sum_j \vec{f}_{ij}^n$, $\vec{f}_{ij}^n = -dU^n/d\vec{r}_{ij}$, $\vec{f}_i^t = \sum_j \vec{f}_{ij}^t$, $\vec{f}_i^d = -b^n\vec{v}_i$, b^n is the damping coefficient, and the sums over j include disks that are in contact with disk i. For the rotational degrees of freedom, we have

$$I_i\frac{d\vec{\omega}_i}{dt} = \vec{\tau}_i - b^t\vec{\omega}_i, \tag{5}$$

where $I_i = m\sigma_i^2/8$ is the moment of inertia for disk i, b^t is the rotational damping coefficient, and

$$\vec{\tau}_i = \frac{1}{2}\sum_j \vec{r}_{ij} \times \vec{F}_{ij}^t \tag{6}$$

is the torque on disk i. We chose b^n and b^t so that the dynamics for the translational and rotational degrees of freedom are in the overdamped limit.

After generating MS packings using these two protcols, we measure the contact number $z = N_c/N'$, where N_c is the total number of contacts in the system, shear stress anisotropy, and normal stress difference of the MS packings. For these measurements, we recursively remove rattler disks with fewer than three contacts for frictionless disks or fewer than two contacts for frictional disks.

3 Results

In this section, we first describe our results for the average contact number and packing fraction of MS packings generated via isotropic compression and simple shear. We then explain why the distribution of the shear stress anisotropy differs for compression and shear jammed packings. We also develop a protocol where we unjam shear jammed packings and then re-jam them via isotropic compression and a protocol where we unjam compression jammed packings and then re-jam them via applied shear strain. We then compare the contact network and stress anisotropy of the original jammed packings and the re-jammed packings, and show that the disk positions of the re-jammed packings are nearly identical to those for the original jammed packings. We find small differences in the stress state of the original jammed packings and the rejammed ones, but these differences are smaller than the fluctuations obtained by enumerating all of the normal and tangential force solutions for a given jammed packing consistent with force and torque balance.

3.1 Packing fraction and contact number

In Fig. 2, we show (for $N = 128$) that the contact number $\langle z_J\rangle$ and packing fraction $\langle \phi_J\rangle$ at jamming onset are similar for compression and shear jammed packings over the full range of friction coefficients μ. (The relative deivations are
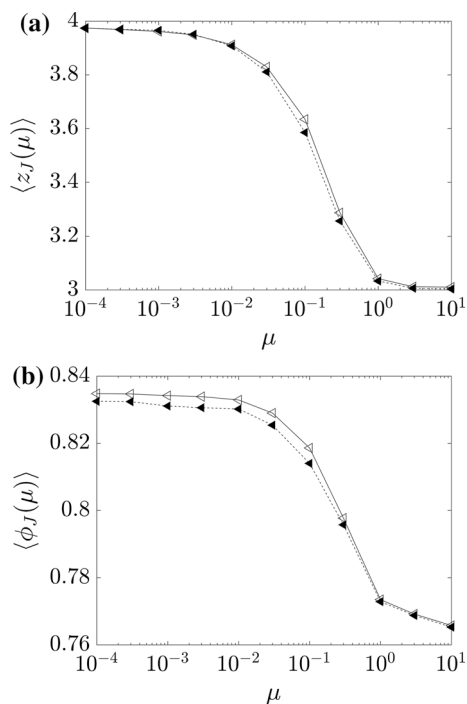
Fig. 2 Average **a** contact number $\langle z_J \rangle$ and **b** packing fraction $\langle \phi_J \rangle$ at jamming onset for MS packings generated via simple shear (filled triangles; dotted lines) and isotropic compression (open triangles; solid lines) plotted versus the static friction coefficient μ for $N = 128$ bidisperse frictional disks. The averages were calculated over more than 50 independent MS packings at each μ (color figure online)
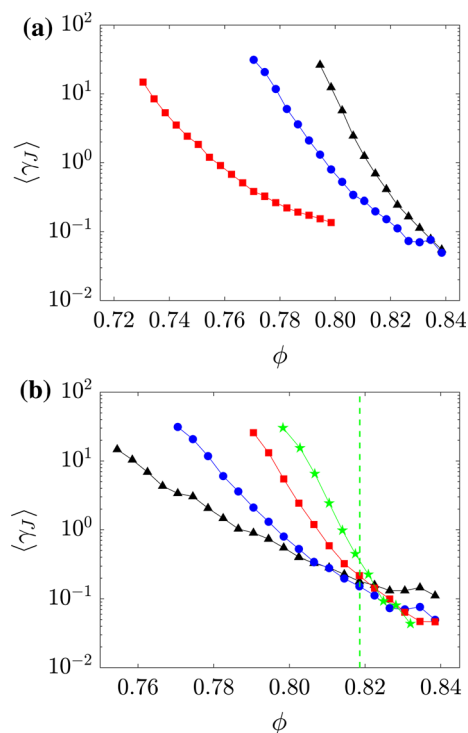

Fig. 3 Average total shear strain $\langle \gamma_J \rangle$ required to jam a collection of disks with **a** $N = 32$ as a function of packing fraction ϕ for several friction coefficients, $\mu = 0$ (black triangles), 0.1 (blue circles), and 1.0 (red squares) and for **b** $\mu = 0.1$ and several system sizes, $N = 16$ (black triangles), 32 (blue circles), 64 (red squares), and 128 (green stars). The vertical dashed line indicates $\langle \phi_J \rangle$ for compression jammed packings with $\mu = 0.1$ and $N = 64$

less than 0.5%.) The data for $\langle z_J \rangle$ and $\langle \phi_J \rangle$ for the isotropic compression protocol in Fig. 2a, b were generated at shear strain $\gamma = 0$. We find the same results when compression jammed packings are generated at different values of γ. For both protocols, we find that $z \approx 4$ in the small-μ limit and $z \approx 3$ in the large-μ limit, as found previously in numerical studies of frictional disks [5]. The average packing fraction $\langle \phi_J \rangle \approx 0.835$ in the small-μ limit and ≈ 0.765 in the large-μ limit. The crossover between the low- and high-friction behavior in the contact number and packing fraction again occurs near $\mu_c \approx 0.1$ for both protocols. This crossover value of μ is similar to that found previously in compression jammed frictional disk packings [5, 17].

The average packing fraction at jamming onset is slightly smaller for shear jammed packings compared to that for compression jammed packings. This small difference in packing fraction stems from differences in the compression and shear jamming protocols. For each initial condition i, we generate a compression jammed packing with ϕ_J^i. Then, for each i, we generate a series of unjammed configurations with $\phi_\alpha^i < \phi_J^i$ and shear them until they jam at γ_J. To obtain $\langle \phi_J \rangle$ for the shear jamming protocol, we average ϕ_α^i over i and α for all systems that jammed. This protocol for generating shear jammed packings is thus biased towards finding MS

packings with packing fractions lower than those found for isotropic compression. Despite this, the packing fraction at jamming onset $\langle \phi_J(\mu) \rangle$ for the two protocols differs by less than 0.5% over the full range of μ.

Prior results for isotropically compressed packings of spheres in three spatial dimensions [5] have shown that $\langle z_J(\mu) \rangle$ and $\langle \phi_J(\mu) \rangle$ show qualitatively the same behavior as the results for shear and compression jammed disk packings in Fig. 2. For packings of frictional spheres, $\langle z_J(\mu) \rangle$ varies between 4 and 6, and $\langle \phi_J(\mu) \rangle$ varies between 0.55 and 0.64, with a transition from frictional to frictionless behavior around $\mu_c \sim 0.1$.

In Fig. 3, we show the average shear strain $\langle \gamma_J \rangle$ required to find a jammed packing starting from an initially unjammed packing using the shear jamming protocol as a function of packing fraction. In panel (a), we plot $\langle \gamma_J \rangle$ versus ϕ for several friction coefficients. The average strain increases with decreasing packing fraction and the range of packing fractions over which a shear jammed packing can be obtained shifts to lower values with increasing friction coefficient. In panel (b), we show $\langle \gamma_J \rangle$ versus ϕ at $\mu = 0.1$ and several system sizes. We find that the slope $d\langle \gamma_J \rangle / d\langle \phi_J \rangle$ increases

with increasing system size. For the $\mu = 0.1$ data in panel (b), we expect $\langle \gamma_J \rangle$ to become vertical near $\phi \approx 0.82$, which is $\langle \phi_J(\mu) \rangle$ for compression jammed packings, in the large-system limit. The system-size dependence of $\langle \gamma_J \rangle$ is similar to that found for packings of frictionless disks [3]. Thus, we predict that the range of packing fraction over which shear jamming occurs to shrink with increasing system size. In particular, we expect shear jamming to occur over a narrow range of packing fraction near $\langle \phi_J(\mu) \rangle$ obtained from isotropic compression in the large-system limit.

3.2 Stress anisotropy of compression and shear jammed packings

In previous studies, we showed that a significant difference between shear and compression jammed packings of frictionless disks is that shear jammed packings possess a non-zero average shear stress anisotropy $\langle \hat{\Sigma}_{xy} \rangle > 0$, whereas compression jammed packings possess $\langle \hat{\Sigma}_{xy} \rangle = 0$. We find similar behavior for MS packings of frictional disks. In Fig. 4, we show the distribution of shear stress anisotropy $P(\hat{\Sigma}_{xy})$ for packings with three friction coefficients $\mu = 0, 0.1$, and 1.0 using the isotropic compression and shear jamming protocols. For the isotropic compression protocol, $P(\hat{\Sigma}_{xy})$ is a Gaussian distribution with zero mean, whereas $\hat{\Sigma}_{xy} > 0$ for packings generated via simple shear (in a single direction). The stress anisotropy distributions $P(\hat{\Sigma}_{xy})$ for simple shear are Weibull distributions with shape and scale factors that depend on μ [26]. In Fig. 5, we show the corresponding averages of the shear stress anisotropy distributions. We find that $\langle \hat{\Sigma}_{xy} \rangle = 0$ for all μ for

Fig. 5 Average shear stress anisotropy $\langle \hat{\Sigma}_{xy} \rangle$ at jamming onset for MS packings generated via simple shear (filled triangles) and isotropic compression (open triangles) plotted versus the static friction coefficient μ for $N = 128$. The error bars indicate the standard deviation in $P(\hat{\Sigma}_{xy})$ for each protocol

packings generated using isotropic compression. In contrast, for packings generated via simple shear, $\langle \hat{\Sigma}_{xy} \rangle \approx 0.13$ [27] for $\mu \to 0$ and $\langle \hat{\Sigma}_{xy} \rangle$ increases with μ until reaching $\langle \hat{\Sigma}_{xy} \rangle \approx 0.25$ in the large-μ limit. Since the normal stress difference $\hat{\Sigma}_N$ does not couple to simple shear strain, $P(\hat{\Sigma}_N)$ is a Gaussian distribution with an average normal stress difference $\hat{\Sigma}_N = 0$ for both compression and shear jammed packings for all μ. (See Appendix 1.)

We showed in previous studies [15] that MS packings of frictionless disks occur in geometrical families in the packing fraction ϕ and shear strain γ plane. For frictionless disks, geometrical families are defined as MS packings with the same network of interparticle contacts, with different, but related fabric tensors. The packing fractions of MS packings in the same geometrical family are related via $\phi = \phi_0 + A(\gamma - \gamma_0)^2$, where $A > 0$ is the curvature in the ϕ-γ plane, and ϕ_0 is the minimum value of the packing fraction at strain $\gamma = \gamma_0$ [16]. The parameters A, ϕ_0, and γ_0 vary from one geometrical family to another. See Appendix 2 for motivation for the parabolic form of geometrical families of disk packings in the ϕ-γ plane.

Using a general work-energy relationship for packings undergoing isotropic compression and simple shear, we showed [19] that for packings of frictionless disks, the shear stress anisotropy can be obtained from the dilatancy, $d\phi_J/d\gamma$:

$$\hat{\Sigma}_{xy} = -\frac{1}{\phi}\frac{d\phi_J}{d\gamma}. \tag{7}$$

The isotropic compression protocol can sample packings with alternating signs of $d\phi_J/d\gamma$ (and thus $\hat{\Sigma}_{xy} > 0$ and < 0), whereas the shear jamming protocol can only sample packings with $d\phi_J/d\gamma < 0$ (and thus $\hat{\Sigma}_{xy} > 0$). We expect similar behavior for packings of frictional disks, however, it is more difficult to identify single geometrical famailies. First, Eq. 7 does not account for sliding contacts, and thus geometrical
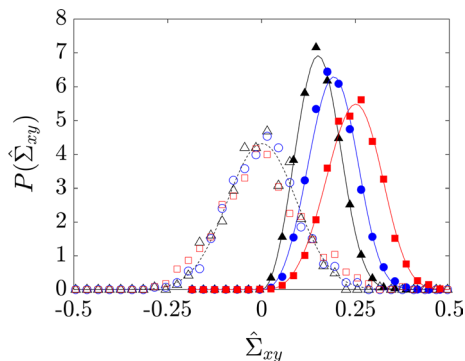

Fig. 4 Probability distributions of the shear stress anisotropy $\hat{\Sigma}_{xy}$ for packings generated via isotropic compression (open symbols) and simple shear (filled symbols). For both packing-generation protocols, we show distributions for $N = 64$ and friction coefficients $\mu = 0$ (triangles), 0.1 (circles), and 1.0 (squares). The distributions were obtained from more than 10^3 independently generated jammed packings. The dashed line is a Gaussian distribution with zero mean and standard deviation $\Delta \sim 0.1$ and the solid lines are Weibull distributions with scale and shape parameters $\lambda \sim 0.17$ and $k \sim 3.0$, $\lambda \sim 0.21$ and $k \sim 3.5$, and $\lambda \sim 0.27$ and $k \sim 3.9$ from left to right
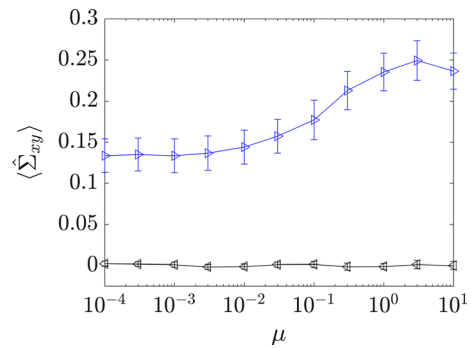
families must be defined over sufficiently small strain intervals such that interparticle contacts do not slide. In addition, for each MS packing of frictional disks in a given geometrical family, there is an ensemble of solutions for the normal and tangential forces [20], not a unique solution, as for the normal forces in packings of frictionless disks. The extent to which packings with the same contact networks (and particle positions) can possess different shear stress anisotropies will be discussed in more detail in Sect. 3.3 below.

3.3 Unjam and rejam compression and shear jammed packings

In Sect. 3.1, we showed that compression and shear jammed packings have similar contact number $\langle z_J(\mu) \rangle$ and packing fraction $\langle \phi_J(\mu) \rangle$ over the full range of μ. However, in Sect. 3.2, we demonstrated that $\langle \hat{\Sigma}_{xy} \rangle = 0$ for compression jammed packings and $\langle \hat{\Sigma}_{xy} \rangle > 0$ for shear jammed packings. Does this significant difference in the stress state of MS packings occur because the packings generated via isotropic compression are fundamentally different from those generated via simple shear?

To address this question, we consider two new protocols—protocol *A*, where we decompress each shear jammed packing, releasing all of the frictional contacts, and then recompress each one until each jams, and protocol *B*, where we shear unjam each compression jammed packing, releasing all of the frictional contacts, and then shear each one until each jams. The goal is to study protocols that allow the system to move away from a given jammed packing in configuration space, removing all of the frictional contacts, and determine to what extent the system can recover the original jammed packing using either compression or shear. We compare the particle positions, shear stress anisotropy, and contact mobility for the original and re-jammed packings. If there is no difference between the original jammed and re-jammed packings, all MS packings can be generated via compression or shear. For protocols *A* and *B*, we will focus on systems with $N = 16$ and $\mu = 0.1$, but we find similar results for systems with larger N and different μ.

In Fig. 6a, we illustrate protocol *A*. We decompress each shear jammed packing at fixed γ by $\Delta\phi \sim 10^{-8}$ that corresponds to the largest overlap, so that none of the particles overlap and all of the tangential displacements are set to zero. We then recompress each packing by $\Delta\phi$ in one step and perform energy minimization. In Table 1, we show that out of the original 8925 shear jammed packings, protocol *A* returned 99% compression rejammed packings with the same contact networks as the original shear jammed packings and only 1% of the compression rejammed packings possessed different contact networks. None of the packings were unjammed after applying protocol *A*. Even though the
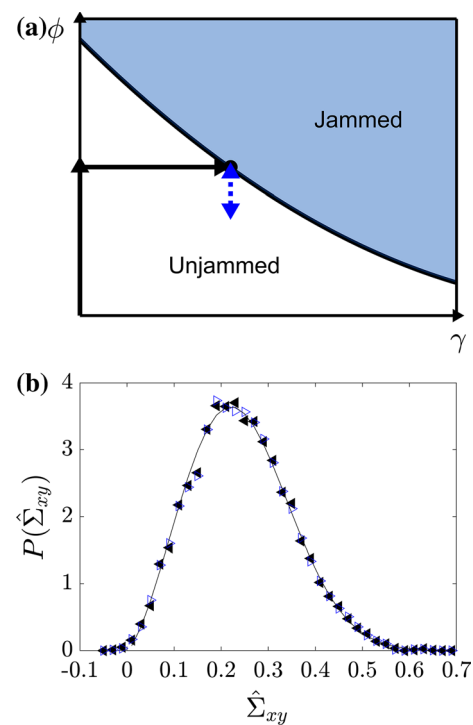

Fig. 6 **a** Illustration of protocol *A* where we first generate a shear jammed packing (solid black lines), then decompress the shear jammed packing by $\Delta\phi$ and recompress it by $\Delta\phi$ to jamming onset (blue dashed line). **b** Probability distribution of the shear stress anisotropy $P(\hat{\Sigma}_{xy})$ for the original shear jammed packings (leftward filled triangles) and those generated using protocol *A* (open rightward triangles) for systems with $N = 16$ and $\mu = 0.1$. The solid line is a Weibull distribution with scale and shape parameters $\lambda \sim 0.27$ and $k \sim 2.5$, respectively (color figure online)

memory of the mobility distribution of the original shear jammed configuration is erased using protocol *A*, we show in Fig. 6b that the distributions of the shear stress anisotropy $P(\hat{\Sigma}_{xy})$ are very similar for the original shear jammed and compression rejammed packings. (We do not include the small number of rejammed packings with different contact networks and the unjammed packings in the distributions $P(\hat{\Sigma}_{xy})$.) In particular, both the compression rejammed packings and the original shear jammed packings possess $\hat{\Sigma}_{xy} > 0$, and thus the distributions have nonzero means, $\langle \hat{\Sigma}_{xy} \rangle > 0$. This result implies that there is not a fundamental difference between shear and compression jammed configurations, since the isotropic compression protocol can generate "shear jammed" configurations.

We now consider a related protocol where we shear unjam compression jammed packings and then apply simple shear to rejam them. In Fig. 7a, we illustrate protocol *B*. We first generate an ensemble of compression jammed packings. Compression jammed packings can jam on either side of the parabolic geometrical families $\phi_J(\gamma)$; roughly half
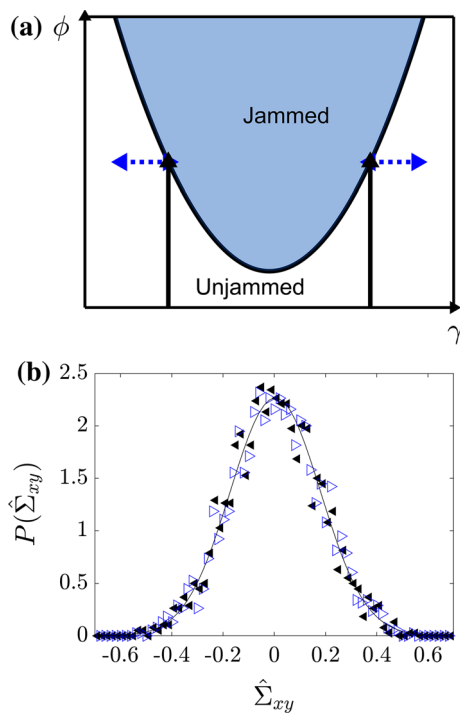
(a) ϕ

Jammed

Unjammed

γ

(b)

$P(\hat{\Sigma}_{xy})$

$\hat{\Sigma}_{xy}$

Fig. 7 **a** Illustration of protocol *B* where we first generate compression jammed packigns (solid black lines). The compression jammed packings possess either $d\phi_J/d\gamma < 0$ (left) or $d\phi_J/d\gamma > 0$ (right). For packings with $d\phi_J/d\gamma < 0$, we apply simple shear to the left by $\Delta\gamma$ to unjam them and then rejam them by applying $\Delta\gamma$ to the right (dashed blue lines on the left). For packings with $d\phi_J/d\gamma > 0$, we apply simple shear to the right by $\Delta\gamma$ to unjam them and then rejam them by applying $\Delta\gamma$ to the left (dashed blue lines on the right). **b** Probability distribution of the shear stress anisotropy $P(\hat{\Sigma}_{xy})$ for the original compression jammed packings (leftward filled triangles) and those generated using protocol *B* (rightward open triangles) for systems with $N = 16$ and $\mu = 0.1$. The solid line is a Gaussian distribution with zero mean and standard deviation $\Delta \sim 0.2$ (color figure online)

with $d\phi_J/d\phi < 0$ and half with $d\phi_J/d\phi > 0$. For packings with $d\phi_J/d\phi < 0$, we shear by $\Delta\gamma \sim 10^{-8}$ in the negative strain direction to unjam the packing. For packings with $d\phi_J/d\phi > 0$, we shear by $\Delta\gamma \sim 10^{-8}$ in the positive strain direction to unjam the packing. In both cases, to unjam the system, we apply simple shear strain in extremely small increments $\delta\gamma = 10^{-12}$, with each followed by energy minimization, until $U/N < U_{\text{tol}}$. Note that for protocol *A*, it is straightforward to identify the largest particle overlap and then decompress the system until there are no overlaps and the system becomes unjammed. However, in protocol *B*, we seek to unjam compression jammed packings by applying simple shear strain, and we do this by applying simple shear strain in small increments to reduce the total potential energy below U_{tol}. (The sensitivity of our results on U_{tol} will be discussed in Appendix 3.) After unjamming the packing in protcol B, we reset the tangential displacements at each nascent contact to zero. We then rejam the packings by applying

the total accumulated shear strain $\Delta\gamma$ in a single step in the opposite direction to the original one, which allows the system to return to the same total strain, and perform energy minimization.

In Table 1, we show that out of the original 1987 compression jammed packings, protocol *B* returned 96% shear rejammed packings with the same contact networks as the original compression jammed packings and only 4% shear rejammed packings with different contact networks. None of the packings generated using protocol *B* were unjammed. As shown in Fig. 7b, the distribution $P(\hat{\Sigma}_{xy})$ of shear stress anisotropies is nearly identical for the original jammed packings and the rejammed packings. In both cases, $P(\hat{\Sigma}_{xy})$ is a Gaussian distribution with zero mean. This result emphasizes that isotropic stress distributions can be generated using a shear jamming protocol (when we consider shear jamming in both the positive and negative strain directions).

We now compare directly the structural and mechanical properties of the original shear jammed packings and those generated using protocol *A* and the original compression jammed packings and those generated using protocol *B*. We calculate the root-mean-square (rms) deviations in the particle positions,

$$\Delta r = \sqrt{N^{-1} \sum_{i=1}^{N} \left(\vec{r}_i^{A,B} - \vec{r}_i^{SJ,CJ} \right)^2},\qquad(8)$$

and shear stress anisotropy,

$$\Delta\hat{\Sigma}_{xy} = \sqrt{\left(\hat{\Sigma}_{xy}^{A,B} - \hat{\Sigma}_{xy}^{SJ,CJ} \right)^2},\qquad(9)$$

between the original shear jammed (SJ) packings and the packings generated using protocol *A* and the original compression jammed (CJ) packings and the packings generated using protocol *B*. In Fig. 8a, we show the frequency distribution of the deviations in the particle positions Δr for systems with $N = 16$ and $\mu = 0.1$. $\langle \Delta r \rangle \sim 2 \times 10^{-12}$ is extremely small, near numerical precision. Thus, the shear jammed packings and those generated via protocol *A* have nearly identical disk positions, and the compression jammed packings and those generated via protocol *B* have nearly identical disk positions.

We perform a similar comparison for the stress anisotropy (for systems with $N = 16$ and $\mu = 0.1$) in Fig. 8b. Even though the disk positions are nearly identical between the shear jammed and compression re-jammed packings, the typical rms deviations in the stress anisotropy $\langle \Delta\hat{\Sigma}_{xy} \rangle$ are finite. The distribution $\Delta\hat{\Sigma}_{xy}$ for the rms deviations in stress anisotropy between shear jammed packings and compression rejammed packings has a peak near $10^{-2.5}$ (open triangles). The stress anisotropy fluctuations are nonzero because packings of frictional disks with
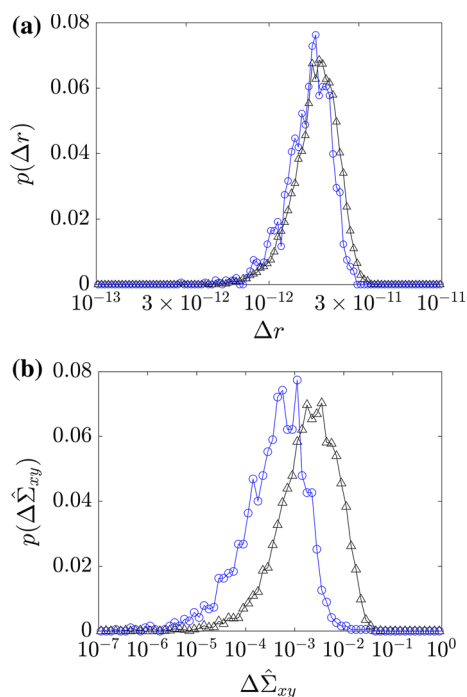
Fig. 8 a The frequency distribution $p(\Delta r)$ of the root-mean-square deviations in the positions of the disks between shear jammed packings and those generated using protocol *A* (triangles) and between compression jammed packings and those generated using protocol *B* (circles). **b** The frequency distribution $p(\Delta \hat{\Sigma}_{xy})$ of the root-mean-square deviations in the stress anisotropy between shear jammed packings and those generated using protocol *A* (triangles) and between compression jammed packings and those generated using protocol *B* (circles). For the data in both panels, $N = 16$ and $\mu = 0.1$

Fig. 9 a The frequency distribution of the mobility $p(\xi)$, where $\xi = f_{ij}^t / \mu f_{ij}^n$ for each contact between disks *i* and *j*, for shear jammed packings (open triangles) and compression re-jammed packings (open circles) with $N = 16$ and $\mu = 0.1$. **b** $p(\xi)$ for compression jammed packings (open triangles) and shear re-jammed packings (open circles) with $N = 16$ and $\mu = 0.1$. The filled symbols indicate the frequency of contacts that slid with $f_{ij}^t = \mu f_{ij}^n$

the *same* particle positions can have multiple solutions for the tangential forces as shown using the force network ensemble [28]. We find similar results for the differences in the stress anisotropy between the compression jammed packings and the shear re-jammed packings, however, the fluctuations are an order of magnitude smaller with $\langle \Delta \hat{\Sigma}_{xy} \rangle \sim 10^{-3.5}$. In contrast, when $\mu = 0$, we find that $\langle \Delta \hat{\Sigma}_{xy} \rangle \sim 10^{-7}$ (nearly four orders of magnitude smaller) when comparing shear jammed packings and packings generated via protocol *A* with $\Delta r < 10^{-12}$.

We also compare the distributions of the mobility at each contact $\xi = F_{ij}^t / \mu F_{ij}^n$ for the shear jammed packings and the compression re-jammed packings, as well as the compression jammed packings and the shear re-jammed packings. In Fig. 9a, we show that the original shear jammed packings have a significant number of contacts that are near sliding with $\xi \sim 1$ and a smaller fraction with $\xi \sim 10^{-3}$. However, the compression re-jammed packings have essentially no sliding contacts, and instead most contacts possess $\xi \sim 10^{-3}$. Thus, we find that the jamming protocol can have a large effect on the contact mobility distribution. We find that applying successive shear strains
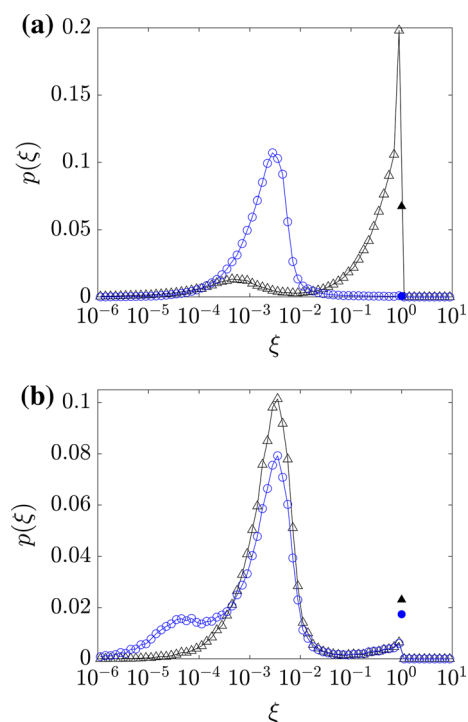
for sufficiently large strains (as is done for shear jammed packings) is able to generate many contacts near sliding. To our knowledge, our study is one of the first to show that shear jammed packings possess more contacts near the sliding threshold than compression jammed packings.

In Fig. 9b, we show $P(\xi)$ for the original compression jammed packings and the shear re-jammed packings. These distributions are similar with a small fraction of sliding contacts and an abundance of contacts with $\xi \sim 10^{-3}$. For $\mu > 10^{-2}$, previous studies have shown that compression jamming does not allow tangential displacements to accumulate so that the tangential forces can approach the sliding threshold [29]. For protocol *B*, where we shear unjam the compression jammed packings, and then shear re-jam them, the applied strain is sufficiently small that the tangential displacements do not accumulate and allow the tangential forces to approach the sliding threshold. This result is consistent with the fact that the stress anisotropy fluctuations between compression jammed and shear re-jammed packings are smaller compared to the stress anisotropy fluctuations between shear jammed and compression re-jammed packings.

Table 1 (first row) Comparison of the contact networks (CN) for the original shear jammed (SJ) packings and compression rejammed packings. (second row) Comparison of the contact networks for the original compression jammed (CJ) packings and shear rejammed packings

SJ	Same CN	Different CN	Unjammed
8925	8875	50	0
CJ	Same CN	Different CN	Unjammed
1987	1899	88	0

4 Conclusion and future directions

In this article, we used discrete element modeling simulations to compare the structural and mechanical properties of jammed packings of frictional disks generated via isotropic compression versus simple shear. We find that several macroscopic properties, such as the average contact number $\langle z_J \rangle$ and packing fraction $\langle \phi_J \rangle$ at jamming onset, are similar for both packing-generation protocols. For both protocols, $\langle z_J(\mu) \rangle$ varies from 4 to 3 in the low- and high-friction limits with a crossover near $\mu_c \approx 0.1$. $\langle \phi_J(\mu) \rangle$ varies from ~ 0.835 to 0.76 in the low- and high-friction limits with a similar crossover value of μ_c.

The average stress state of mechanically stable (MS) packings generated via isotropic compression is different than that for MS packings generated via simple shear. The average stress anisotropy $\langle \hat{\Sigma}_{xy} \rangle > 0$ for MS packings generated via shear, but $\langle \hat{\Sigma}_{xy} \rangle = 0$ for packings generated via isotropic compression. Isotropic compression can sample MS packings with both signs of $\hat{\Sigma}_{xy}$, whereas simple shear (in one direction) samples packings with only one sign of the stress anisotropy.

To investigate in detail the differences in the stress state of MS packings generated via simple shear and isotropic compression, we developed two additional protocols. For protocol A, we decompress shear jammed packings so that the frictional contacts are removed and then re-compress them to jamming onset. For protocol B, we shear unjam MS packings generated via isotropic compression so that the frictional contacts are removed, and then shear re-jam them. These studies address an important question—to what extent can protocols A and B recover the contact networks and stress states of the original jammed packings. We find that even though protocols A and B can recover the particle positions (and contact networks) of the original jammed packings, the rejammed and original jammed packings have small, but signficant differences in the stress anisotropy, e.g. $\Delta \hat{\Sigma}_{xy} \sim 10^{-3.5}$–$10^{-2.5}$ for systems with $\mu = 0.1$.

To understand the stress fluctuations of frictional packings with nearly identical particle positions, we carried out preliminary studies of the null space solutions for force and torque balance on all grains using the contact networks from the MS packings generated via isotropic compression [30]. For each packing of frictional disks, force and torque balance on all grains can be written as a matrix equation $\mathcal{A}_{lm} F_m = 0$, where $\mathcal{A}_{lm}$ is a $3N \times 2N_c$ constant matrix determined by the contact network and F_m is a $2N_c \times 1$ vector that stores the to-be-determined normal and tangential force magnitudes f_{ij}^n and f_{ij}^t at each contact. For frictional disk packings, the system is underdetermined with $3N < 2N_c$. Using a least-squares optimization approach [31], we solve for the normal and tangential force magnitudes such that $f_{ij}^n > 0$, and $f_{ij}^t \leq \mu f_{ij}^n$.

The stress anisotropy frequency distribution $p(\hat{\Sigma}_{xy})$ from the null space solutions for an example compression jammed packing (with $N = 16$ and $\mu = 0.1$) is shown in Fig. 10. We find that the DEM-generated solutions belong to the set of null space solutions, but there are many more. In particular, the width of $p(\hat{\Sigma}_{xy})$ from the null space solutions is much larger than the width of the distribution of the stress anisotropy obtained for the given compression jammed packing from protocol B. We performed similar calculations of the null space solutions for all compression jammed packings. In Fig. 11, we show the frequency distribution of the standard devivations $\sigma_{\hat{\Sigma}_{xy}}$ of stress anisotropy from the null space solutions over all of the compression jammed packings. We find that the width of the fluctuations of the stress anisotropy from the null space
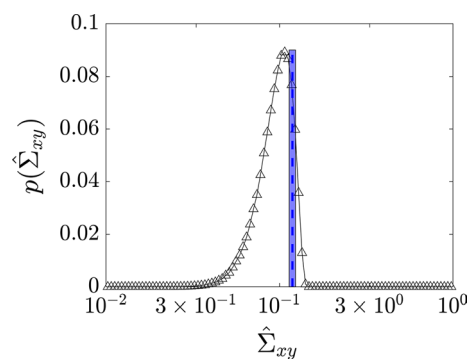

Fig. 10 The frequency distribution of the shear stress anisotropy $p(\hat{\Sigma}_{xy})$ calculated from the null space solutions for a single compression jammed packing (open triangles). The vertical dashed line at $\hat{\Sigma}_{xy} \approx 0.12$ is the stress anisotropy of the given compression jammed packing and the shaded blue region (with width 5×10^{-3}) indicates the fluctuations in the stress anisotropy obtained by comparing the compresssion jammed and shear rejammed packings from the DEM simulations
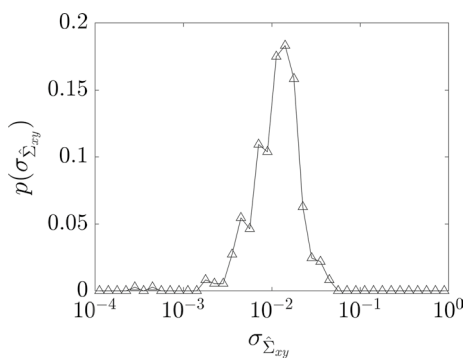
Fig. 11 The frequency distribution $p(\sigma_{\hat{\Sigma}_{xy}})$ of the standard deviation of the stress anisotropy from the null space solutions for each of the compression jammed packings. The peak in $p(\sigma_{\hat{\Sigma}_{xy}})$ is $\sigma_{\hat{\Sigma}_{xy}} \approx 10^{-2}$

solutions for a given packing are comparable to fluctuations of the stress anisotropy over all compression jammed contact networks using DEM. In future studies, we will carry out similar calculations to understand how the fluctuations in the stress anisotropy from the null space scale with system size N and friction coefficient μ. For example, we will investigate over what range of N and μ are the null space stress aniostropy fluctuations larger than the stress anisotropy fluctuations from varying contact networks. Addressing this question will allow us to predict the differences in the structural and mechanical properties of jammed packings of frictional particles that arise from the packing-generation protocols, such as isotropic compression and both continuous and cyclic pure and simple shear [32].

Compliance with ethical standards

Conflict of interest The authors declare that they have no conflict of interest.

Appendix 1: Normal stress difference in jammed and rejammed packings

In this Appendix, we describe the results for the normal stress difference for jammed packings of frictional disks generated via simple shear and isotropic compression. In Fig. 12, we show the probability distribution $P(\hat{\Sigma}_N)$ of the normal stress difference for both shear and comrpession jammed packings with $N = 64$ at $\mu = 0$, 0.1, and 1.0. Simple shear and isotropic compression do not strongly couple to $\hat{\Sigma}_N$ and thus we find that $P(\hat{\Sigma}_N)$ is a Gaussian distribution centered at zero with a width that depends on μ. We also calculated $\Delta\hat{\Sigma}_N$, which is the rms deviation in the normal stress difference between the rejammed and original jammed packings for protocols A and B. In Fig. 13, we show that (as for
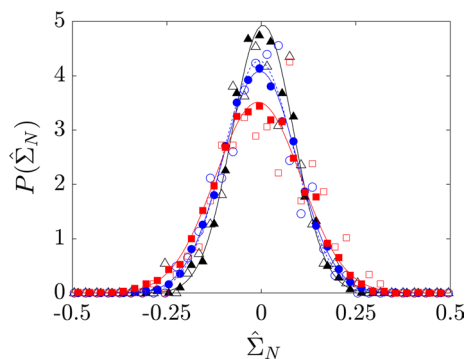

Fig. 12 Probability distribution of the normal stress difference $P(\hat{\Sigma}_N)$ for jammed packings generated via isotropic compression (open symbols) and simple shear (closed symbols) for $N = 64$ and friction coefficients $\mu = 0$ (triangles), 0.1 (circles), and 1.0 (squares). The distributions were obtained from more than 10^3 independently generated jammed packings. The solid lines are Gaussian distributions with zero mean and standard deviations $\Delta \approx 0.091$, 0.093, and 0.114 for $\mu = 0$, 0.1, and 1.0, respectively
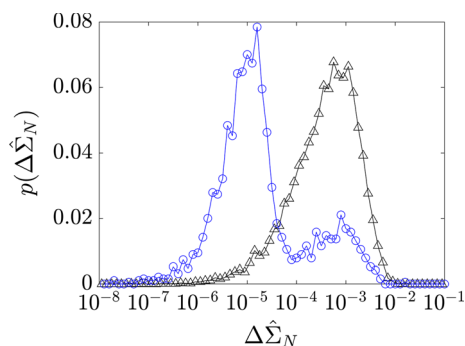

Fig. 13 The frequency distribution $p(\Delta\hat{\Sigma}_N)$ of the root-mean-square deviation in the normal stress difference between shear jammed packings and those generated using protocol A (triangles) and between compression jammed packings and those generated using protocol B (circles)

the stress anisotropy), the rms deviation in the normal stress difference $\Delta\hat{\Sigma}_N$ is typically larger between shear jammed packings and compression rejammed packings, compared to that between compression jammed packings and shear rejammed packings.

Appendix 2: Parabolic geometrical families

Geometrical families are collections of jammed packings that share the same interparticle contact network at different values of the packing fraction at jamming onset ϕ_J and either pure or simple shear strain γ. In this Appendix, we present a derivation of the relation between ϕ_J and γ for a simple example of jammed packings of two hard disks (one small disk with diameter σ_s and one large disk with diameter σ_l) undergoing pure shear strain $\gamma = \ln\left(\frac{L_x}{L_y}\right)$ in a box with side walls with lengths L_x and L_y in the x- and y-directions. We first express the box lengths $L_x = \sigma_{ls}(1 + \cos\theta)$ and $L_y = \sigma_{ls}(1 + \sin\theta)$ in terms of the angle θ between the horizontal axis of the box and $\vec{r}_{ij}$ connecting the centers of the disks. See Fig. 14a. Thus, the pure shear strain satisfies

(a)

L_y θ j i L_x

(b)

Fig. 14 **a** Illustration of a jammed packing of two bidisperse disks i and j in a simulation cell with side lengths L_x and L_y in the x- and y-directions and periodic boundary conditions. θ gives the angle between the center-to-center separation vector $\vec{r}_{ij}$ and the x-axis. **b** The packing fraction at jamming onset ϕ_J versus the pure shear strain γ for packings of two bidisperse disks obtained from Eq. B4 (solid blue line) and DEM simulations (open triangles). The jammed packing fraction ϕ_0 and pure shear strain γ_0 at the minimum and the curvature A of the parabola are given in the main text (color figure online)

$$\gamma = \ln\left(\frac{1 + \cos\theta}{1 + \sin\theta}\right). \tag{B1}$$

In addition, we can write the jammed packing fraction as

$$\phi_J = \frac{\phi_1}{(1 + \cos\theta)(1 + \sin\theta)}, \tag{B2}$$

where

$$\phi_1 = \frac{\pi(\sigma_s^2 + \sigma_l^2)}{(\sigma_s + \sigma_l)^2}. \tag{B3}$$

Using Eqs. B1 and B2, we can eliminate the dependence on θ and write ϕ_J in terms of γ:

$$\phi_J = \phi_1\left[\sqrt{2} - 2\cosh\left(\frac{\gamma}{2}\right)\right]^2. \tag{B4}$$

Equation B4 is similar to a parabola, which can be seen by expanding it in powers of $\gamma - \gamma_0$ about the minimum at $\gamma_0 = 0$ and retaining terms up to $(\gamma - \gamma_0)^2$:

$$\phi_J = \phi_0 + A(\gamma - \gamma_0)^2, \tag{B5}$$

where $\phi_0 = (6 - 4\sqrt{2})\phi_1$ and $A = \left(1 - \frac{\sqrt{2}}{2}\right)\phi_1$. We carried out discrete element method simulations to generate jammed packings at each value of the pure shear strain γ for two bidisperse hard disks. The DEM results for $\phi_J(\gamma)$ agree with the analytical result as shown in Fig. 14. For small systems, a single geometrical family can exist over a wide range of strain. Also, for pure shear in small systems, the parabolic geometrical family is centered on $\gamma = 0$. In contrast, for simple shear of two hard bidisperse disks (in fixed wall boundary conditions), the parabolic geometrical family is not centered on $\gamma = 0$ as shown in Fig. 15.
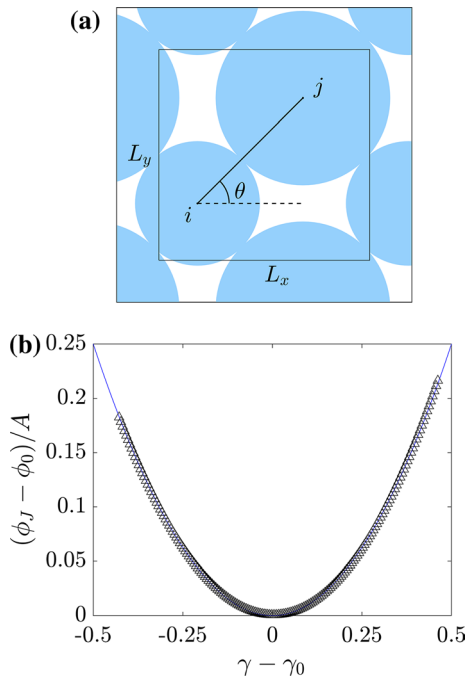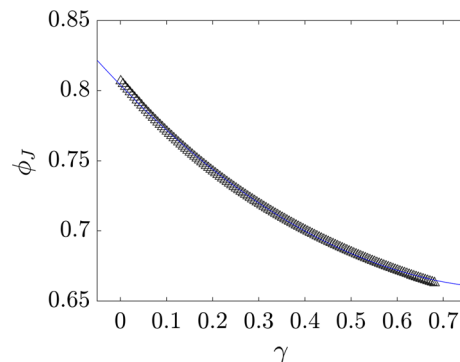
Fig. 15 The packing fraction at jamming onset ϕ_J versus the simple shear strain γ for packings of two bidisperse disks obtained from DEM simulations (open triangles). We also show a fit to a parabolic form, $\phi_J = \phi_0 + A(\gamma - \gamma_0)^2$, where $\phi_0 \approx 0.49$, $A \approx 0.34$, and $\gamma_0 \approx 1.03$ (solid blue line) (color figure online)

Appendix 3: Sensitivity of results on numerical parameters of packing-generation protocols

In this Appendix, we investigate how the ability to generate the original jammed packing from the rejamming protocols A and B depends on parameters associated with the packing-generation protocols. When determining the packing fraction at jamming onset, we seek particle configurations for which the total potential per particle U/N is nonzero, but small, i.e. $U_{tol} < U/N < 2U_{tol}$ and $U_{tol} = 10^{-16}$ for the results provided in the main text. To better understand the sensitivity of our results on U_{tol}, we calculate the frequency distribution for rms deviations in the positions between shear jammed packings and compression rejammed packings as a function of U_{tol}. For $U_{tol} = 10^{-16}$, $p(\Delta r)$ is narrow with a peak near $\Delta r \approx 10^{-12}$ as shown in Fig. 16. However, for $U_{tol} = 10^{-14}$ and 10^{-12}, $p(\Delta r)$ broadens dramatically, with non-zero probability between $\Delta r = 10^{-11}$ and 10^{-7}. These results emphasize that it is more difficult to recover the original jammed packing for packings that are over-compressed because over-compressed packings are further from the unjammed state, increasing the likelihood that the system can find a pathway to another jammed configuration during the re-jamming process.

Does the stress anisotropy for shear jammed and compression re-jammed packings (or for compression jammed and shear re-jammed packings) differ for systems at $\mu = 0$? In general, the stress anisotropy distributions are similar for jammed and re-jammed packings, but the precise values of the stress anisotropy can differ for each original jammed packing and its rejammed counterpart. We find that the average value of the stress anisotropy difference $\langle \Delta \hat{\Sigma}_{xy} \rangle \approx 10^{-5}$ (between shear jammed and compression re-jammed packings) for $\mu = 0.1$, but $\langle \Delta \hat{\Sigma}_{xy} \rangle \approx 10^{-7.5}$ is much lower for $\mu = 0$. (See Fig. 17.) In contrast to the results for $\mu > 0$,
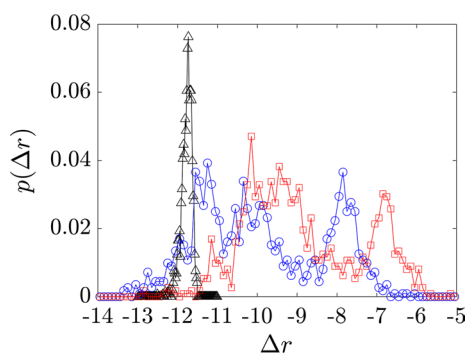
$\langle \Delta \hat{\Sigma}_{xy} \rangle$ for $\mu = 0$ scales to zero with the degree to which the simulations can maintain force balance.
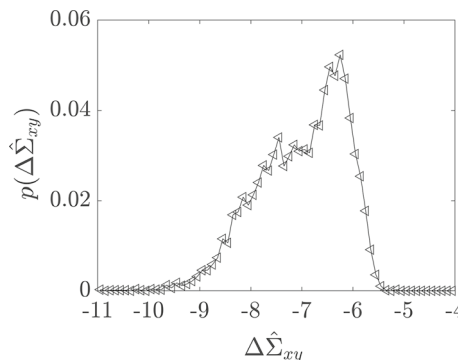
References

Fig. 17 The frequency distribution $p(\Delta \hat{\Sigma}_{xy})$ of the root-mean-square deviations in the stress anisotropy between shear jammed packings and those generated using protocol A for $N = 16$ and $\mu = 0$

1. O'Hern, C.S., Silbert, L.E., Liu, A.J., Nagel, S.R.: Jamming at zero temperature and zero applied stress: the epitome of disorder. Phys. Rev. E **68**, 011306 (2003)
2. Makse, H.A., Johnson, D.L., Schwartz, L.M.: Packing of compressible granular materials. Phys. Rev. Lett. **84**, 4160 (2000)
3. Bertrand, T., Behringer, R.P., Chakraborty, B., O'Hern, C.S., Shattuck, M.D.: Protocol dependence of the jamming transition. Phys. Rev. E **93**, 012901 (2016)
4. Bililign, E.S., Kollmer, J.E., Daniels, K.E.: Protocol dependence and state variables in the force-moment ensemble. Phys. Rev. Lett. **122**, 038001 (2019)
5. Silbert, L.E.: Jamming of frictional spheres and random loose packing. Soft Matter **6**, 2918–2924 (2010)
6. Miskin, M.Z., Jaeger, H.M.: Evolving design rules for the inverse granular packing problem. Soft Matter **10**, 3708–3715 (2014)
7. Inagaki, S., Otsuki, M., Sasa, S.: Protocol dependence of mechanical properties in granular systems. Eur. Phys. J. E **34**, 124 (2011)
8. Ciamarra, M.P., Nicodemi, M., Coniglio, A.: Recent results on the jamming phase diagram. Soft Matter **6**, 2871–2874 (2010)
9. Majmudar, T.S., Behringer, R.P.: Contact force measurements and stress-induced anisotropy in granular materials. Nature **435**, 1079 (2005)
10. Bi, D., Zhang, J., Chakraborty, B., Behringer, R.P.: Jamming by shear. Nature **480**, 355 (2011)
11. Zhang, J., Majmudar, T., Behringer, R.: Force chains in a two-dimensional granular pure shear experiment. Chaos: an interdisciplinary journal of nonlinear science **18**, 041107 (2008)
12. Zhang, J., Majmudar, T.S., Tordesillas, A., Behringer, R.P.: Statistical properties of a 2D granular material subjected to cyclic shear. Granul. Matter **12**, 159–172 (2010)
13. Kondic, L., Goullet, A., O'Hern, C.S., Kramar, M., Mischaikow, K., Behringer, R.P.: Topology of force networks in compressed granular media. EPL (Europhys. Lett.) **97**, 54001 (2012)
14. Gao, G.-J., Blawzdziewicz, J., O'Hern, C.S.: Frequency distribution of mechanically stable disk packings. Phys. Rev. E **74**, 061304 (2006)

Fig. 16 Frequency distribution $p(\Delta r)$ of the root-mean-square deviations in the positions of the disks between shear jammed packings and those generated using protocol A for $U_{tol} = 10^{-16}$ (black triangles), 10^{-14} (blue circles), and 10^{-12} (red squares), N=16 and μ=0.1 (color figure online)

15. Gao, G.-J., Blawzdziewicz, J., O'Hern, C.S.: Geometrical families of mechanically stable granular packings. Phys. Rev. E **80**, 061303 (2009)

16. Chen, S., Bertrand, T., Jin, W., Shattuck, M.D., O'Hern, C.S.: Stress anisotropy in shear-jammed packings of frictionless disks. Phys. Rev. E **98**, 042906 (2018)

17. Papanikolaou, S., O'Hern, C.S., Shattuck, M.D.: Isostaticity at frictional jamming. Phys. Rev. Lett. **110**, 198002 (2013).

18. Song, C., Wang, P., Makse, H.A.: A phase diagram for jammed matter. Nature **453**, 629 (2008)

19. Shen, T., Papanikolaou, S., O Hern, C.S., Shattuck, M.D.: Statistics of frictional families. Phys. Rev. Lett. **113**, 128302 (2014)

20. Shaebani, M.R., Unger, T., Kertész, J.: Extent of force indeterminacy in packings of frictional rigid disks. Phys. Rev. E **79**, 052302 (2009)

21. Handin, J.: On the Coulomb Mohr failure criterion. J. Geophys. Res. **74**, 5343–5348 (1969)

22. Cundall, P.A., Strack, O.D.: A discrete numerical model for granular assemblies. Geotechnique **29**, 47–65 (1979)

23. Xu, N., Blawzdziewicz, J., O Hern, C.S.: Random close packing revisited: ways to pack frictionless disks. Phys. Rev. E **71**, 061306 (2005)

24. Silbert, L.E., Ertas, D., Grest, G.S., Halsey, T.C., Levine, D.: Geometry of frictionless and frictional sphere packings. Phys. Rev. E **65**, 031304 (2002)

25. Silbert, L.E., Ertas, D., Grest, G.S., Halsey, T.C., Levine, D., Plimpton, S.J.: Granular flow down an inclined plane: Bagnold scaling and rheology. Phys. Rev. E **64**, 051302 (2001)

26. Clark, A.H., Shattuck, M.D., Ouellette, N.T., O'Hern, C.S.: Role of grain dynamics in determining the onset of sediment transport. Phys. Rev. Fluids **2**, 034305 (2017)

27. Peyneau, P.E., Roux, J.N.: Frictionless bead packs have macroscopic friction, but no dilatancy. Phys. Rev. E **78**, 011307 (2008)

28. Tighe, B.P., Snoeijer, J.H., Vlugt, T.J., van Hecke, M.: The force network ensemble for granular packings. Soft Matter **6**, 2908–2917 (2010)

29. Shundyak, K., van Hecke, M., van Saarloos, W.: Force mobilization and generalized isostaticity in jammed packings of frictional grains. Phys. Rev. E **75**, 010301 (2007)

30. Vinutha, H.A., Sastry, S.: Force networks and jamming in shear-deformed sphere packings. Phys. Rev. E **99**, 012123 (2019)

31. Coleman, T.F., Li, Y.: A reflective Newton method for minimizing a quadratic function subject to bounds on some of the variables. SIAM J. Optim. **6**, 1040–1058 (1996)

32. Royer, J.R., Chaikin, P.M.: Precisely cyclic sand: self-organization of periodically sheared frictional grains. Proc. Natl. Acad. Sci. **112**, 49–53 (2015)

Publisher's Note Springer Nature remains neutral with regard to jurisdictional claims in published maps and institutional affiliations.